buildings

MDPI

Article

Machine Learning-Based Evaluation of Tower Foundation Frost Jacking in the Marginal Permafrost of Northeast China

Juncen Lin [1,2], Guoyu Li [1,2,*], Kai Gao [1,2], Dun Chen [1,2], Yapeng Cao [1,2] and Alexander N. Fedorov [3]

[1] Key Laboratory of Cryospheric Science and Frozen Soil Engineering, Northwest Institute of Eco-Environment and Resources, Chinese Academy of Sciences, Lanzhou 730000, China; linjuncen@nieer.ac.cn (J.L.); gaokai@nieer.ac.cn (K.G.); chendun@lzb.ac.cn (D.C.); caoyapeng@lzb.ac.cn (Y.C.)
[2] University of Chinese Academy of Sciences, Beijing 100049, China
[3] Melnikov Permafrost Institute, Siberian Branch of the Russian Academy of Sciences (SB RAS), Yakutsk 677010, Russia; fedorov@mpi.ysn.ru
* Correspondence: guoyuli@lzb.ac.cn

Abstract

Rapid localized permafrost degradation heightens geological risk and threatens the long-term stability of transmission towers in cold regions. Based on systematic field investigations of 336 towers in the marginal permafrost of Northeast China, thirteen conditioning factors were incorporated to evaluate five machine learning models (Random Forest, XGBoost, LightGBM, CatBoost, Logistic Regression) for foundation frost jacking susceptibility assessment, with SHapley Additive exPlanations (SHAP) and Geographical Detector (GeoDetector) used to quantify factor contributions and interactions. Results show that differential frost jacking poses the greatest structural hazard. Peat-rich wetland geohydrological settings constitute the highest-risk terrain for foundation uplift. Random Forest achieved the highest area under the curve of 0.987 and showed competitive performance across multiple evaluation metrics. Ground ice content was the most influential predictor, followed by land cover, soil type, and surface water. Ice content and land cover exhibited the strongest explanatory power (q = 0.78). These findings provide a quantitative and interpretable basis for frost-jacking susceptibility assessment and preliminary engineering screening within the investigated transmission corridor.

Keywords: risk evaluation; frost jacking; machine learning; permafrost degradation; distress

1. Introduction

Permafrost degradation poses increasing challenges to infrastructure stability in cold regions, particularly in marginal zones. Among these, Northeast China is one of the most representative and vulnerable regions, where permafrost is especially susceptible to environmental perturbations [1–3]. This region has experienced rapid climatic warming [4], resulting in widespread permafrost degradation along the margins of the Xing'an permafrost (XAP) region [5,6]. Meanwhile, the pipelines and the highways within the engineering corridor have further accelerated permafrost degradation [7–9]. Notably, frost heaving-related damage to transmission tower foundations has received comparatively limited attention.

Transmission tower foundations play a critical role in ensuring the safety of overhead power systems. However, their complex physical interactions with surrounding permafrost significantly increase the risk of frost heave-induced uplift driven by ice segregation within a frost depth [10]. For example, during the construction and upgrading of 110–500 kV

Check for updates

Academic Editor: Fabrizio Gara

Received: 3 September 2026
Revised: 11 October 2026
Accepted: 12 October 2026
Published: 16 October 2026

Copyright: © 2026 by the authors. Licensee MDPI, Basel, Switzerland. This article is an open access article distributed under the terms and conditions of the Creative Commons Attribution (CC BY) license.

overhead transmission lines in northern West Siberia, uplift displacements of tower foundations exceeding 2 m have been reported [11]. In addition, investigations conducted in Russia in the late 1980s documented cases of tower collapse caused by differential frost jacking [12]. In the permafrost regions of the Qinghai–Tibet Plateau, foundations have also experienced increasingly severe uplift during operation [13–15]. In Northeast China, tower foundations embedded in permafrost are frequently uplifted. Ice-rich permafrost commonly persists beneath wetland surfaces, largely maintained by the insulating effects of vegetation cover and thick organic peat layers [16]. However, the construction of tower foundations disturbs vegetation and topsoil structure, alters local hydrological conditions, and disrupts the surface thermal–hydrological equilibrium [17]. These variations lead to an accelerating thawing of ice adfrozen to foundation walls and a reduction in uplift resistance. Despite the widespread occurrence and engineering significance of this problem, systematic investigations into its spatial patterns and predictive assessment remain limited, particularly in permafrost wetland environments.

Field investigations are fundamental for accurately understanding and evaluating engineering conditions along infrastructure corridors [18]. Cao et al. [19] identified frost jacking and freeze–thaw damage of protective caps as the dominant distress types in Northeast China and proposed corresponding mitigation measures. Guo et al. [20] investigated 130 towers along the Qinghai–Tibet transmission line and reported that vertical displacement was primarily characterized by settlement with a rate of 25%, which was attributed to creep in warm and ice-rich permafrost. Existing studies have largely focused on large-scale linear infrastructures [8,21], whereas investigations of point-based transmission towers remain limited. Moreover, the quantitative relationships between foundation distress and environmental factors are still insufficiently understood.

Machine learning (ML) methods, with their strengths in data integration and feature selection, are effective in identifying key driving factors and enabling robust risk prediction [22]. In recent years, ML has been widely applied to susceptibility assessment and risk zoning of permafrost-related hazards, such as thaw settlement and thermokarst landslides [23–25]. Moreover, a recent study has evaluated thaw settlement susceptibility using multiple environmental factors and identified high-risk sections along the Qinghai–Tibet Highway and Railway [26]. Zhang et al. [27] applied Logistic Regression and Support Vector Machine models incorporating climatic, geological, and engineering factors to assess risks in transitional sections of the Qinghai–Tibet Railway. These studies also compared model performance, offering valuable references for hazard assessment in permafrost regions. However, despite their predictive capability in key influencing factors, most ML models are limited by their "black-box" nature, raising concerns regarding interpretability. To address this restriction, the SHapley Additive exPlanations (SHAP) method, based on game theory, has emerged as a powerful tool for enhancing model interpretability by quantifying the contribution of individual features to prediction outcomes [28]. It enables the identification of dominant environmental controls for improved hazard assessment [25,29].

In this context, the present study focuses on developing a quantitative susceptibility assessment for transmission-tower foundation frost jacking based on a systematic field dataset from the marginal permafrost of Northeast China. Based on field investigation of 336 transmission towers, the types and spatial distribution of foundation distress are characterized. Five ML models are compared to quantify the nonlinear contributions of environmental and engineering variables. The SHAP method is employed to interpret frost jacking prediction results. In addition, the Geographical Detector (GeoDetector) method is applied to assess the explanatory power of each factor from the perspective of spatial heterogeneity, thereby complementing the limitations of ML in spatial attribution analysis.

2. Materials and Methods

2.1. Investigation Area

The XAP region in Northeast China is located within a mid-latitude transitional permafrost belt, characterized by dense forests and widespread *Carex tato* wetlands (Figure 1) [30]. In this region, permafrost occurs predominantly as sporadic and isolated patches, which are highly susceptible to climate warming and intensified human activities. The engineering corridor in the study area primarily consists of the China–Russia crude oil pipelines (CRCOPs) and National Highway G111, which runs between Da and Xiao Xing'anling Mountains. The field survey was conducted along the routes extending from Jagdaqi to Mohe and Xing'an, respectively. The surveyed transmission towers are distributed across regions dominated by sporadic and isolated permafrost, with 113 and 221 towers identified, respectively, with the remaining two located in non-permafrost regions (Figure 1c). A notable concentration of 131 towers occurs near the Jagdaqi area (Figure 1d). The presence of warm and ice-rich permafrost environments introduces considerable geohazard uncertainties for infrastructure stability (Figure 1e,i).

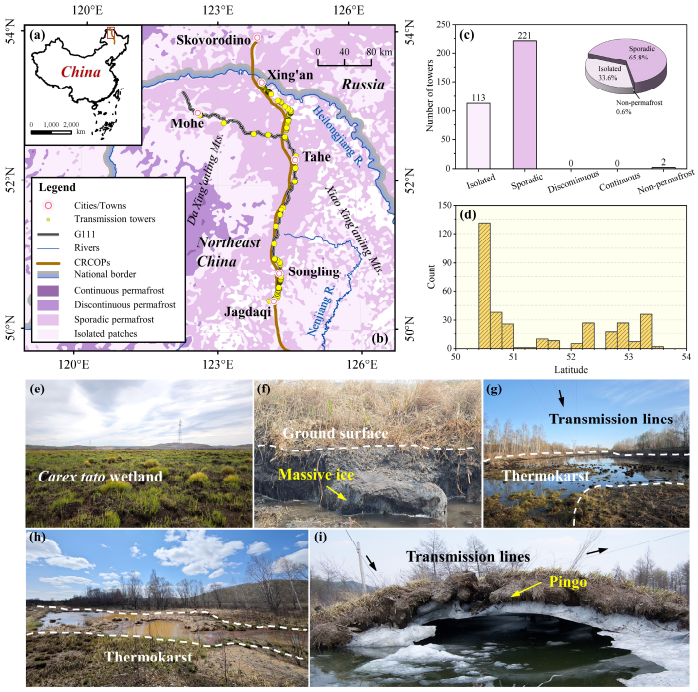


Figure 1. Investigated towers and surrounding environment: (**a**) Location of study area in Northeast China; (**b**) Permafrost distribution extracted from [30]; (**c**) Tower distribution in various permafrost types; (**d**) Tower distribution across different latitudes; (**e**) *Carex tato* wetland in the area; (**f**) Ground ice beneath the wetland; (**g**) Thermokarst along the transmission route; (**h**) Thermokarst in the nature scene; (**i**) Pingo along the transmission route.

2.2. Data Sources

Tower foundation deformation is a multifactorial process. In this study, a total of thirteen variables were incorporated into the analytical framework, including elevation, land cover type, slope, surface water, aspect, surface deformation, annual precipitation (AP), soil type, mean annual air temperature (MAAT), ground ice content, MAGT, foundation width, and base spacing. Herein, climatic variables, including AP and MAAT for 2020, were obtained from the Environmental Meteorology Data Service Platform (http://eia-data.com/, accessed on 25 December 2025). MAGT data were sourced from PANGAEA-Data Publisher for Earth & Environmental Science (https://doi.pangaea.de/10.1594/PANGAEA.888600, accessed on 25 December 2025). A 30-m resolution digital elevation model (DEM)

derived from the Shuttle Radar Topography Mission (SRTM) was adopted (https://dwtkns.com/srtm30m/, accessed on 25 December 2025) and was used to generate topographic factor maps (slope and aspect) in ArcGIS 10.8. Table 1 lists the resolution and source of these datasets. Engineering-related data, including ice content and foundation design parameters, were collected from the Electric Power Research Institute, State Grid Heilongjiang Electric Power Company Limited (Harbin, China). Land cover, soil type, surface water, surface deformation, and geographic coordinates were determined through the site investigations from 2023 to 2024. Finally, the maps of all conditioning factors were produced and exported for subsequent analysis, with the results presented in Figure 2.

Table 1. Derived data source information from various platforms.

Factors	Temporal Resolution	Spatial Resolution	Source
MAAT	Daily	1 km × 1 km	EMDSP
AP	Daily	1 km × 1 km	EMDSP
MAGT	Yearly	1 km × 1 km	PANGAEA
Elevation	/	30 m × 30 m	SRTM

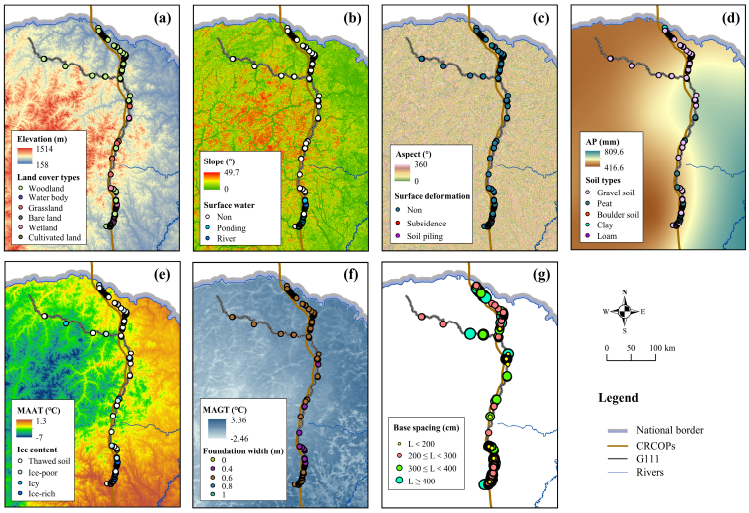


Figure 2. Multi-source data of thirteen factors from the databases and field investigation: (**a**) Elevation and land cover types; (**b**) Slope and surface water; (**c**) Aspect and surface deformation; (**d**) AP and soil types; (**e**) MAAT and Ice content; (**f**) MAGT and foundation width; (**g**) Base spacing.

2.3. Modeling and Methodological Strategy

2.3.1. Field Survey

The present field dataset was developed as a substantial extension of the regional transmission-line survey reported by Cao et al. [19]. The surveys focused on and documented typical characteristics of tower foundation damage (Figure 3). Site-specific conditions, including surface water and soil type, were also verified and recorded. Because no independent stable elevation benchmark was available during the field survey, possible deformation or subsidence of the surrounding ground could not be separated from foundation movement. The measured quantity in this study represents the relative displacement h between the foundation and the adjacent ground surface rather than independently measured absolute foundation uplift. It was calculated as the measured exposed height of the foundation minus the designed exposed height of 20 cm. At the tower level, a tower was labeled as frost-jacked if at least one of its individual foundations exhibited $h > 0$; otherwise, it was labeled as non-frost-jacked. Towers and surrounding environmental features (e.g.,

ponding) were further documented using a DJI Matrice 300 RTK unmanned aerial vehicle (UAV) (DJI-SZ DJI Technology Co., Ltd., Shenzhen, China).

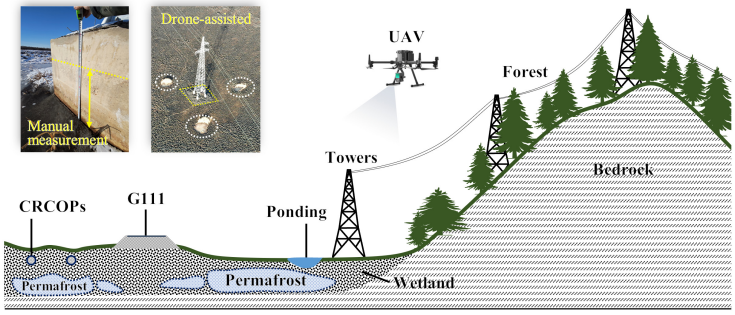


Figure 3. Investigation methodology of transmission lines along the engineering corridor in the XAP region.

2.3.2. ML Models and Evaluation

ML has gained widespread recognition for its application in the assessment and prediction of geohazards and engineering defects [26,31]. The modeling workflow adopted in this study is presented in Figure 4. Five supervised ML models, including Random Forest (RF), XGBoost, LightGBM, CatBoost, and LR, were implemented using the 13 predictors in Section 2.2. RF is an ensemble learning method based on bagging, which improves prediction accuracy and robustness by aggregating multiple decision trees [32]. In contrast, XGBoost, LightGBM, and CatBoost are gradient boosting algorithms that iteratively optimize prediction residuals while incorporating regularization to control model complexity [33–35]. Among them, LightGBM enhances computational efficiency through histogram-based learning and feature bundling, whereas CatBoost effectively handles categorical variables and mitigates overfitting using an ordered boosting strategy. LR was included as a baseline model due to its simplicity and interpretability [36].

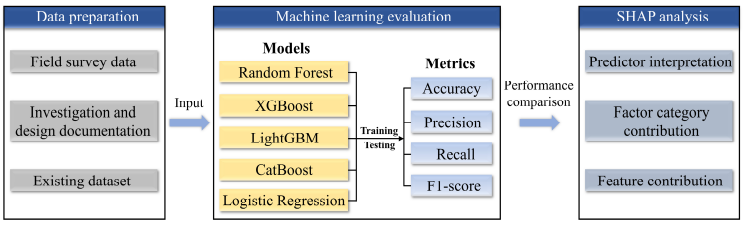


Figure 4. Procedures of ML evaluation and interpretation.

No missing values were identified in the final dataset. Categorical predictors were encoded according to the requirements of the different algorithms. For LR, categorical variables were transformed using one-hot encoding, whereas ordinal encoding was applied to categorical variables for RF, XGBoost, LightGBM, and CatBoost. The complete dataset comprised 336 tower-level samples, including 77 frost-jacked (positive) towers and 259 non-frost-jacked (negative) towers. Using a stratified 70%/30% split with a fixed random seed of 42, the training set contained 54 positive and 181 negative samples, while the test set contained 23 positive and 78 negative samples. Because the investigated towers are distributed along a geographically heterogeneous engineering corridor, the random holdout split was used to evaluate internal predictive performance within the present dataset. This validation scheme does not explicitly eliminate potential spatial dependence between geographically neighboring towers and therefore should not be interpreted as an independent assessment of spatial transferability.

Hyperparameter selection was performed using Bayesian optimization, with classification accuracy as the optimization criterion. Model performance during hyperparameter optimization was assessed using K-fold cross-validation conducted exclusively within the training set. The test set was completely excluded from parameter search, hyperparameter selection, and model selection, and was used only for the final independent evaluation of the optimized models. For RF, n_estimators = 100, max_depth = 10, min_samples_split = 2, min_samples_leaf = 1, and max_features = 'sqrt'. For XGBoost, n_estimators = 100, max_depth = 6, learning_rate = 0.1, subsample = 0.8, and colsample_bytree = 0.8. For LightGBM, n_estimators = 100, max_depth = 6, num_leaves = 31, learning_rate = 0.1, and subsample = 0.8. For CatBoost, iterations = 100, depth = 6, and learning_rate = 0.1. For LR, max_iter = 1000. All machine-learning analyses were conducted in Python 3.10.

The classification performance was assessed using accuracy (A), precision (P), recall (R), F1-score, and receiver operating characteristic (ROC) with its area under the curve (AUC). The definitions of evaluation metrics are provided as follows:

$$A = \frac{TP + TN}{TP + FP + TN + FN} \tag{1}$$

$$P = \frac{TP}{TP + FP} \tag{2}$$

$$R = \frac{TP}{TP + FN} \tag{3}$$

$$F1\text{-}score = 2\frac{P \times R}{P + R} \tag{4}$$

$$TPR = \frac{TP}{TP + FN}, FPR = \frac{FP}{FP + TN} \tag{5}$$

where TP, TN, FP, and FN represent true positive, true negative, false positive, and false negative in the confusion matrix, respectively. TPR denotes the true positive rate, and FPR represents the false positive rate.

To improve model interpretability, the SHAP method was employed to quantify the contribution of each input feature to model predictions [37]. SHAP provides both global and local explanations, enabling the identification and ranking of predictors according to their contributions to model predictions. All SHAP values were computed on training datasets to avoid information leakage and ensure the reliability of interpretation results.

2.3.3. GeoDetector Method

GeoDetector is a statistical method designed to detect spatial stratified heterogeneity and reveal the explanatory power of potential driving factors [38]. This method is currently widely applied in road disease risk assessment [39]. GeoDetector includes four types of detectors, namely the factor detector, interaction detector, risk zone detector, and ecological detector. In this study, the factor detector and interaction detector were employed to investigate the spatial explanatory patterns and combined associations of conditioning factors with tower foundation frost jacking. The factor detector was used to quantify the explanatory power of each conditioning factor on the spatial distribution of foundation distress, while the interaction detector was applied to assess the combined effects of two factors. The explanatory strength is measured using the q-statistic, which ranges from 0 to 1, with higher values indicating stronger explanatory power and more pronounced spatial heterogeneity.

The q-statistic is defined as:

$$q = 1 - \frac{\sum_{h=1}^{L} N_h \sigma_h^2}{N\sigma^2} \quad (6)$$

where $h = 1, \ldots, L$ denotes the stratification of factor X or variable Y; N_h and N represent the number of units in stratum h and the entire area, respectively; σ_h^2 and σ^2 are the variance within stratum h and the entire area, respectively.

The dependent variable Y was tower-level frost-jacking occurrence, coded as 1 for frost-jacked towers and 0 for non-frost-jacked towers. For GeoDetector analysis, elevation, AP, MAAT, and MAGT were discretized into five strata using quantile-based classification. Aspect, slope, and ground ice content were divided into four strata; foundation width and base spacing into five strata; surface deformation and surface water into three strata; soil type into five strata; and land cover into six strata. The significance of the factor-detector q-statistics was evaluated using the standard non-central F test implemented in GeoDetector, with $p < 0.05$ considered statistically significant.

Because GeoDetector results can be sensitive to the discretization of continuous variables, and because overlaying two factors may produce joint strata with relatively small sample sizes, the interaction results were interpreted as exploratory measures of joint explanatory power. No causal or mechanistic inference was made from the magnitude of the joint q-values. Future studies with larger and more spatially balanced datasets should examine the robustness of the interaction results under alternative stratification schemes.

3. Results

3.1. Distress Type and Spatial Distribution

Field investigations identified five main types of distress affecting transmission tower foundations in the permafrost region (Figure 5). The first type is uniform frost jacking despite trapezoidal sloped foundations used to reduce tangential frost heaving force (Figure 5a,b). The relative elevation difference among the foundations is typically less than 10 cm, resulting in low hazard levels. A contrasting type is non-uniform frost jacking, characterized by significant relative elevation differences among individual foundations. This type is most prevalent in permafrost wetlands and poses a pronounced threat to superstructural stability. As shown in Figure 5c, foundations #3 and #4 are significantly higher than #1 and #2, leading to tower tilting and a risk of overturning. In Figure 5d, the frost heave at foundation #1 is notably lower than the other numbers, resulting in severe deformation and cracking of the tower, which was subsequently repaired and reconstructed.

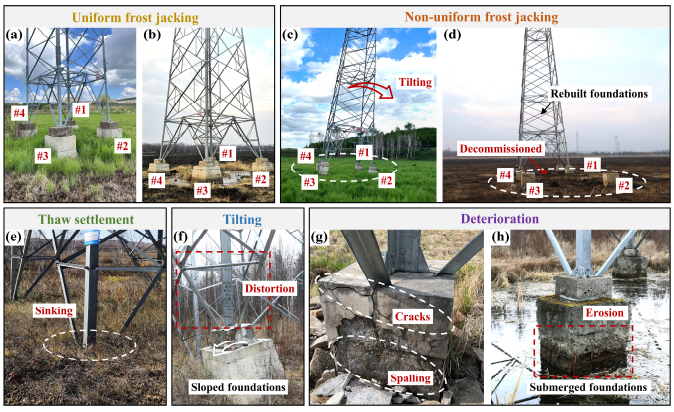


Figure 5. Five types of distress in the transmission tower foundations: (**a**,**b**) Uniform frost jacking; (**c**,**d**) Non-uniform frost jacking; (**e**) Thaw settlement; (**f**) Tilting; (**g**,**h**) Deterioration.

The third type involves overall subsidence of the foundation and its protective cap (Figure 5e), generally exerting minor impacts on towers. The fourth type is tilting of a single foundation, exerted by uneven tangential and horizontal frost-heave forces, which can directly lead to distortion and failure of the superstructure, as shown in Figure 5f. The fifth type is strength deterioration due to reinforced concrete frost cracking (Figure 5g,h), manifested by extensive cracking and surface spalling. In more severe cases, foundations immersed in ponded areas formed by ground settlement exhibit progressive structural deterioration, where prolonged water exposure accelerates erosion of both concrete and internal reinforcement, thereby reducing integrity and bearing capacity. Notably, 60.6% of the frost-jacked foundations were associated with ponded environments, highlighting the critical role of surface water in promoting frost jacking.

Within the study area, the occurrence rates of uniform and non-uniform frost jacking were 14.3% and 8.7%, respectively, as shown in Figure 6. Their spatial distributions are indicated by red and pink dots, respectively, with both types predominantly concentrated in the Jagdaqi-Songling section. The concentration reflects the complex geological conditions and intensified human disturbances along the corridor, which have significantly affected permafrost stability. In contrast, other types of distress occur less frequently. Thaw settlement and tilting are also mainly observed within the same section. The deterioration rate is 5.1%, with concentrated distributions in both the Jagdaqi–Songling and Tahe–Xing'an sections. Overall, the distribution of distress types exhibits regional characteristics and is closely related to the local geological and hydrological conditions.

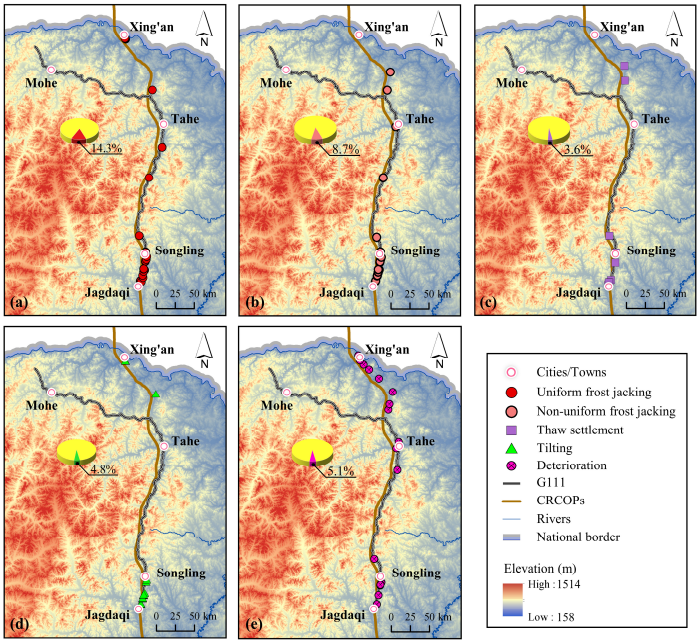


Figure 6. Spatial distribution of distress types in transmission tower foundations: (**a**) Uniform frost jacking; (**b**) Non-uniform frost jacking; (**c**) Thaw settlement; (**d**) Tilting; (**e**) Strength deterioration.

3.2. Statistical Characteristics of Frost Jacking

3.2.1. Comparison Between Frost Jacking and Thaw Settlement

Figure 7 presents the displacement of tower foundations induced by frost jacking and thaw settlement, with n representing the tower number. Uplift-related deformation occurs far more frequently than thaw settlement, with approximately six times as many cases observed. The number of uniform frost-jacking cases (48) exceeds that of non-uniform frost-jacking cases (29) by 19. However, the average magnitude of uniform frost jacking (34.1 cm) is notably smaller than that of non-uniform frost jacking (59 cm). In terms of

average frost jacking amount (AFJA), the non-uniform case exhibits substantially greater displacements, with maximum uplift approaching 160 cm. Meanwhile, the maximum differential displacement reaches 38 cm (with an average of 20.6 cm). Such pronounced displacement gradients can directly compromise structural stability and lead to severe damage to tower systems.

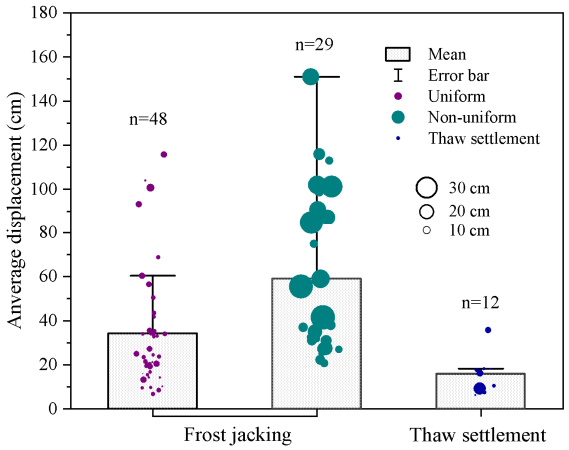


Figure 7. Average displacement and differential amount of frost jacking and thaw settlement.

3.2.2. Association with the Foundation Tilting

Frost jacking-induced tilting of tower foundations represents a critical factor threatening the safety of transmission lines. Figure 8 shows the distribution of AFJA for tilted and non-tilted foundations, with mean values of 63.7 cm and 38.7 cm, respectively. This suggests that higher AFJA is generally associated with an increased likelihood of foundation tilting. Among the tilted foundations, non-uniform frost jacking accounts for approximately 70%, showing its dominant role in inducing tilting. Figure 9 presents the correlation analysis among different types of foundation distress. It is observed that there is a positive correlation only between tilting and non-uniform frost jacking, with a correlation coefficient of 0.37. These results suggest that non-uniform frost jacking is a key contributing factor to foundation tilting, although the moderate correlation also indicates that additional factors may be involved.

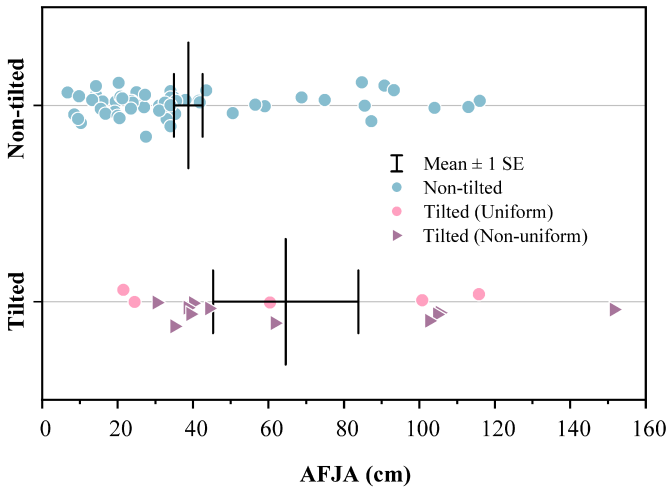


Figure 8. Statistics on tilted and non-tilted foundations subjected to uplift. AFJA denotes the average frost jacking amount of each tower.

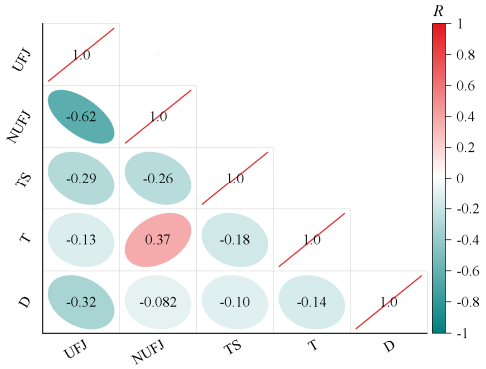


Figure 9. Correlation between various distress types. Notes: Uniform frost jacking (UFJ); Non-uniform frost jacking (NUFJ); Thaw settlement (TS); Tilting (T); Deterioration (D).

3.2.3. Relationship Between Frost Jacking and Foundations

Figure 10 illustrates the statistical relationships between frost heaving and various factors using box plots and heatmap visualization. Frost jacking magnitude *h* is categorized into six levels to show its distribution patterns. As shown in Figure 10a, at a width of 40 cm, the average frost heaving reaches 45.4 cm, while the corresponding values for other widths are 41.8 cm, 80.1 cm, and 47.3 cm, respectively. In addition, foundations with widths of 40 cm and 60 cm are more prevalent, and extreme cases (h > 100 cm) account for 14% and 9%, respectively. Figure 10b shows the relationship between frost heaving and base spacing. The highest h (52.7 cm) occurs at a spacing of 3–4 m. Meanwhile, frost jacking events are more frequent at spacings of 2–3 m and 3–4 m, with 116 and 92 affected foundations, respectively. Among these, the proportions of extreme cases (h > 100 cm) are 14% and 13%, respectively.

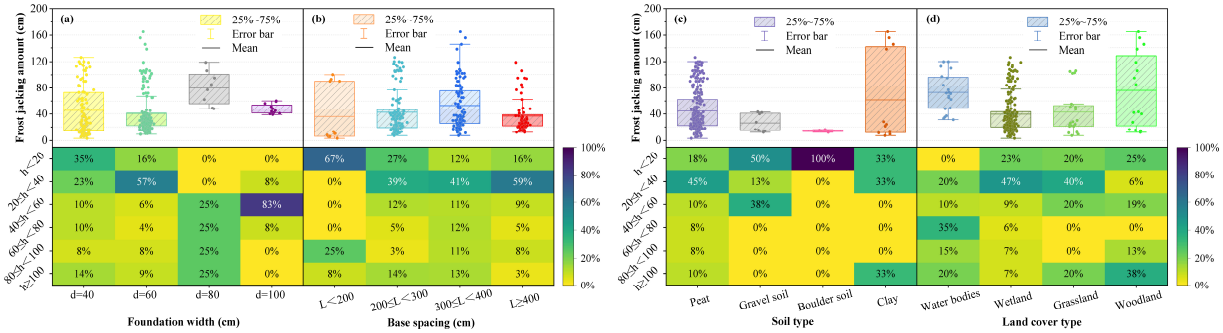


Figure 10. Box plots and heat maps of the relationship between frost heaving and foundations and environmental factors: (**a**) Foundation width; (**b**) Base spacing; (**c**) Soil type; (**d**) Land cover type.

3.2.4. Relationship Between Frost Jacking and Environmental Factors

Figure 10c shows that the largest number of frost jacking occurs in peat soils, with 65 affected towers, whereas only a few cases are observed in gravel soil, boulder soil, and clay (2, 1, and 3 towers, respectively). The average frost heaving is 44.5 cm in peat and 61.5 cm in clay. The relatively high value in clay is associated with a water-rich, fine-grained, and frost-susceptible environment, which can significantly amplify upward force upon freezing. In contrast, although frost heave is also observed in blocky soils, the magnitude remains below 20 cm, substantially lower than in other soil types.

The investigated land cover types include water body, wetland, grassland, and woodland. As shown in Figure 10d, higher average frost heaving appears in the water body (73 cm) and forest land (76.1 cm). Thermokarst ponds surrounding tower foundations accelerate permafrost degradation and enhance the frost process. Notably, 16 foundations exhibit uplift exceeding 1 m in widespread wetlands. Given the extensive distribution

of wetlands, transmission lines inevitably traverse these areas. Along the engineering corridor, a total of 228 foundations experienced frost jacking, with an average magnitude of approximately 40 cm. These patterns highlight the controlling role of environmental heterogeneity in the intensity of frost jacking.

3.3. ML Model Performance Evaluation

3.3.1. Performance Comparison

To quantify the influence of environmental factors on tower foundation damage, five ML models were trained using the 13 predictors described in Section 2.2. The predictive performance was evaluated using ROC curves, as illustrated in Figure 11. All models exhibit strong predictive capability, with the *TPR* increasing rapidly in the low *FPR* region, indicating effective identification of high-risk cases with limited false alarms.

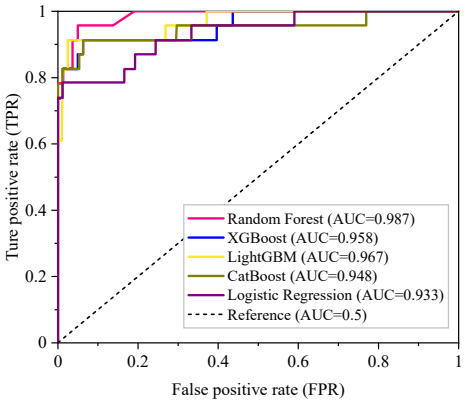


Figure 11. ROC curves and associated AUC of the adopted ML models.

Among them, the RF model achieved the highest AUC value of 0.987. The LightGBM model also performs well, with an AUC of 0.967, followed by XGBoost (AUC = 0.958) and CatBoost (AUC = 0.948), all of which demonstrate stable and reliable predictive performance. In contrast, the LR model yielded the lowest AUC (0.933), with its ROC curve lying below those of all tree-based ensemble models.

Figure 12 compares the performance of five ML models across different evaluation metrics. In this figure, light purple squares represent results on the training set, while dark purple circles indicate performance on the test set. Figure 12a presents the accuracy of each model. Overall, the *A*-values on the training set are consistently higher than those on the test set for all models. Among them, the RF model achieves the highest accuracy on the training set, followed by LightGBM (A = 0.996). On the test set, RF and CatBoost share the highest accuracy, both reaching 0.95, indicating that these two models perform well on this dataset. In contrast, the LR model shows the lowest accuracy on both the training and test sets. Figure 12b compares precision. Although the LR model performs poorly on the training set, with a precision of only 0.904, it achieves a precision of 1 on the test set. The RF model attains the highest precision on both the training and test sets (p = 1). As shown in Figure 12c, the RF model reaches a recall of 1 on the training set, whereas the LR model yields the lowest recall (R = 0.87). RF, XGBoost, LightGBM, and CatBoost demonstrate relatively good recall performance on the test set, all with values of 0.783. Regarding the F1-score, the RF model again performs best on both the training and test sets, with values of 1 and 0.878, respectively, while the LR model performs the worst (Figure 12d).

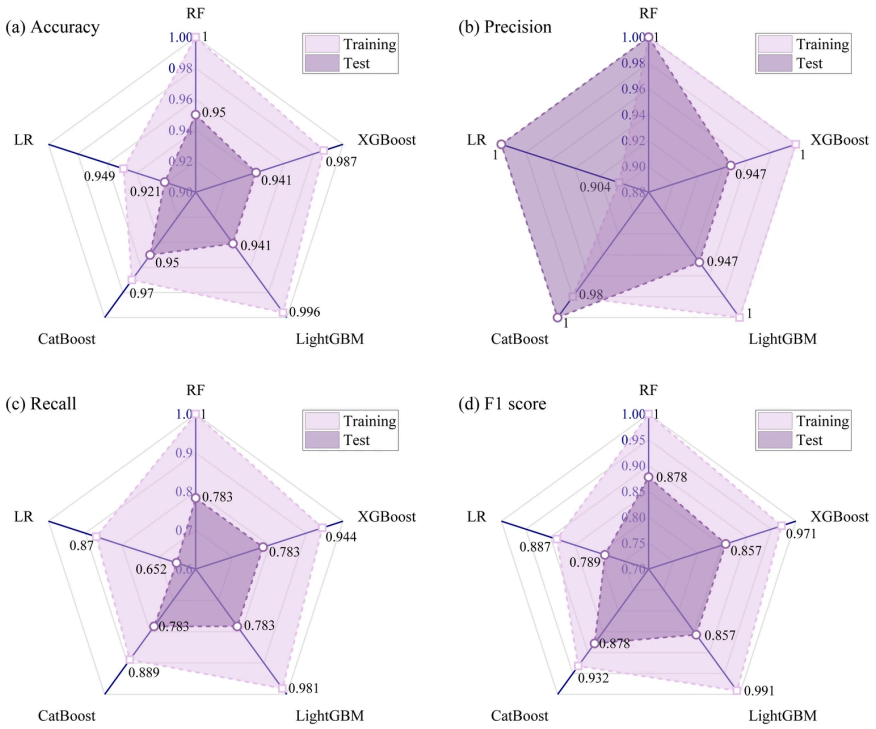


Figure 12. Radar chart of multi-indicator performance comparison of the adopted five algorithms: (**a**) Accuracy; (**b**) Precision; (**c**) Recall; (**d**) F1 score.

Overall, RF achieved the highest observed AUC (0.987) under the adopted train-test split while showing competitive performance across the other evaluation metrics. Therefore, RF was selected for subsequent feature-importance and SHAP analyses because it achieved the highest AUC while maintaining competitive performance across the other evaluation metrics.

It should be noted that the test recall of 0.783 indicates that approximately 21.7% of the positive cases were not identified at the adopted classification threshold. From an engineering perspective, such false-negative predictions are important because potentially frost-jacked towers may be missed during susceptibility screening. Therefore, the present model should be regarded as a supplementary tool for prioritizing field inspection rather than a substitute for engineering investigation and monitoring.

3.3.2. Dominant Predictors Identified by ML

The importance ranking of input features in the RF-based prediction model is shown in Figure 13. It is observed that ice content is the most critical factor influencing frost jacking. An increase in soil ice content corresponds to a greater potential for frost heave. During ice crystal growth, stronger frost heaving forces significantly drive the deformation of tower foundations. Surface cover type ranks second, as it indirectly affects the soil freezing depth and frost heave magnitude by altering the efficiency of heat exchange between the soil and the atmosphere, as well as the pathways of moisture migration. This is followed by surface water and soil type, respectively. Surface water provides a continuous supply of moisture necessary for soil freezing, serving for sustained ice crystal growth and the accumulation of frost heaving forces. Meanwhile, soil type regulates frost heave deformation through its inherent properties, such as particle gradation and pore structure. In addition, Figure 13 shows that the three features with the lowest contribution to the model's predictive performance are surface deformation, aspect, and foundation width.

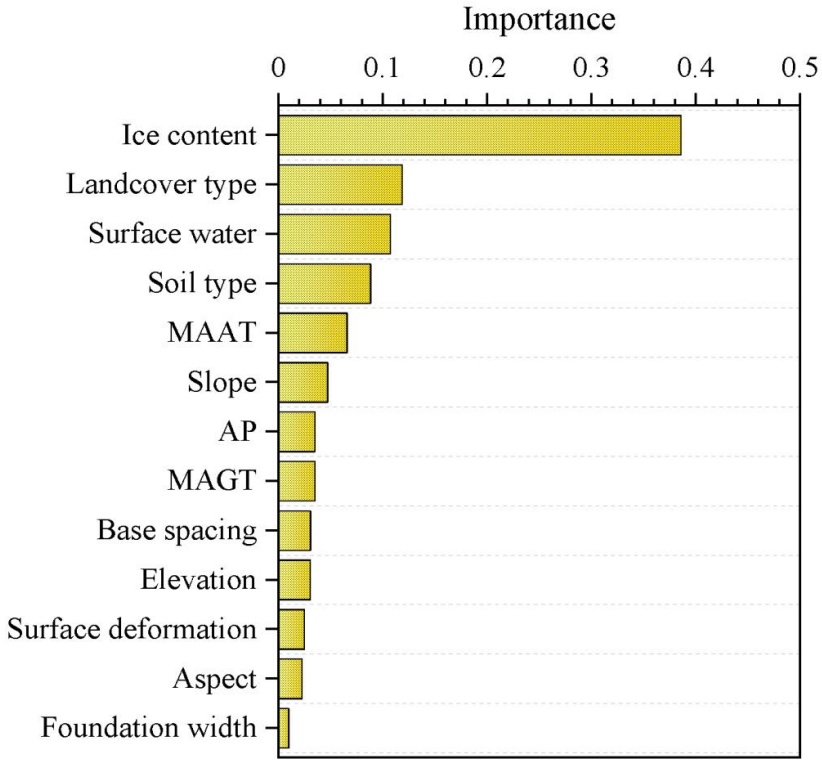


Figure 13. Ranking of predictors' importance.

The SHAP method calculates the marginal contribution of each feature under different combinations by traversing all possible combinations of input features, and then takes the average as the SHAP value for that feature, thereby achieving fair attribution and quantitative evaluation of feature influence. In the SHAP summary plot (Figure 14), features are arranged along the *y*-axis in descending order based on the mean absolute SHAP values. The *x*-axis represents the SHAP value corresponding to each sample, and individual samples are displayed as scatter points, allowing for an intuitive visualization of how variations in feature values influence the prediction results. Global feature importance is obtained by calculating the mean of the absolute SHAP values of each feature across all samples, which effectively reflects the overall impact strength of each feature on the model predictions. A larger mean absolute SHAP value indicates a more dominant role of that feature in predicting tower foundation distress.

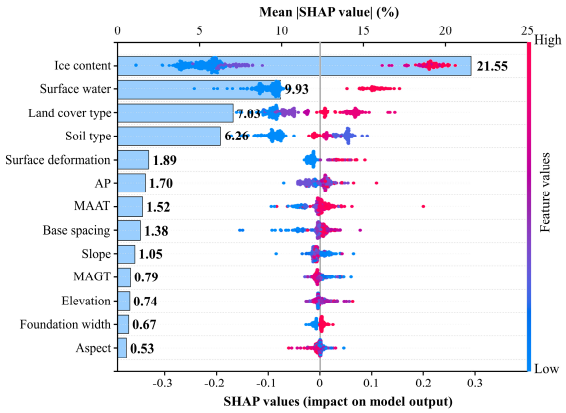


Figure 14. SHAP-based summary plot showing the importance of each predictor by RF.

The prediction results shown in Figure 14 indicate that ice content is the most critical feature, accounting for 21.55% of the total mean absolute SHAP value, and thus plays

the most prominent role in controlling the prediction outcomes. In contrast, aspect has the weakest influence, with a contribution of only 0.53%, making its effect on frost heave prediction negligible. This ranking is generally consistent with the feature importance analysis of the RF model (Figure 13), further confirming the dominant role of ice content in uplift processes. From the relationship between scatter color and SHAP values, red points represent higher feature values, while blue points denote lower feature values. Taking ice content as an example, its SHAP values show a clear increasing trend with rising ice content. The blue points on the far left of Figure 14 correspond to samples of low ice content with negative SHAP values, shifting the model output away from the frost-jacked class. As ice content increases, SHAP values gradually rise to the relatively larger red points on the right, demonstrating that high ice content was associated with positive SHAP values, shifting the model output toward the frost-jacked class.

SHAP dependence plots illustrate the association between individual feature values and their contributions to the RF model output. Figure 15 presents the distribution of SHAP values for key features in frost jacking prediction. In Figure 15a, when the soil is thawed or ice-poor, the SHAP values remain negative. In contrast, icy and ice-rich soil corresponds to positive SHAP values. For tower foundation samples with water supply (Figure 15b), SHAP values are concentrated in the positive range, indicating that surface water contributes positively to the prediction. As shown in Figure 15c,d, wetland and peat-soil categories were predominantly associated with positive SHAP values and shifted the model prediction toward the frost-jacked class. Conversely, woodland and gravel soil show the most pronounced negative contributions, with SHAP values at the lowest levels among all variables.

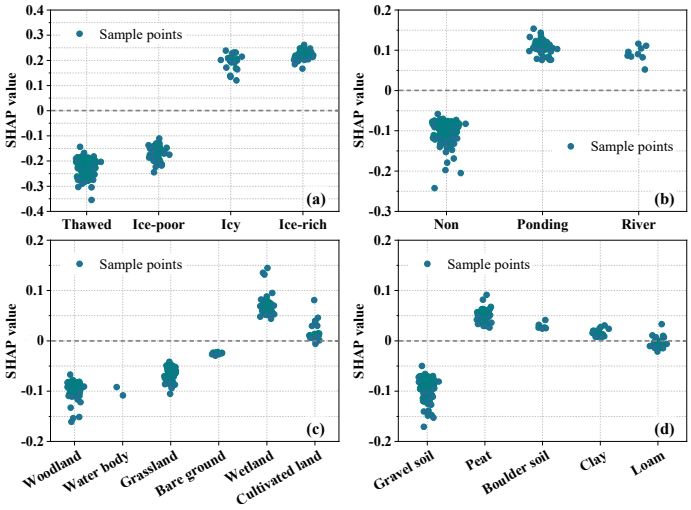


Figure 15. Dependence scatter plots showing the contributions of the first four factors: (**a**) Ice content; (**b**) Surface water; (**c**) Land cover type; (**d**) Soil type.

In summary, wetlands in cold regions represent high-risk areas where typically high ground ice content, abundant surface water, and frost-susceptible soils exist. Field observations further confirm that such environments commonly contain large quantities of ice lenses and fine-grained silt clay [40,41]. Nevertheless, these factors associated with positive SHAP values correspond to more adverse engineering geological conditions for foundation stability.

3.4. Drivers of Foundation Frost Jacking

The results of the factor detection analysis are shown in Figure 16. Except for foundation width, the *p*-values of all other influencing factors are less than 0.05, indicating

that these factors have a statistically significant effect on frost jacking. Among them, ice content has the highest q-value (0.73), making it the most dominant driving factor with the strongest explanatory power. Land cover type (q = 0.68), soil type (q = 0.56), and surface water (q = 0.45) rank second through fourth, respectively. In contrast, slope and base spacing have much lower q-values, at 0.03 and 0.04, respectively, indicating their weak effects. In summary, ice content, surface water, soil type, and land cover type are the key factors affecting frost heave of tower foundations, with ice content playing the most prominent role.

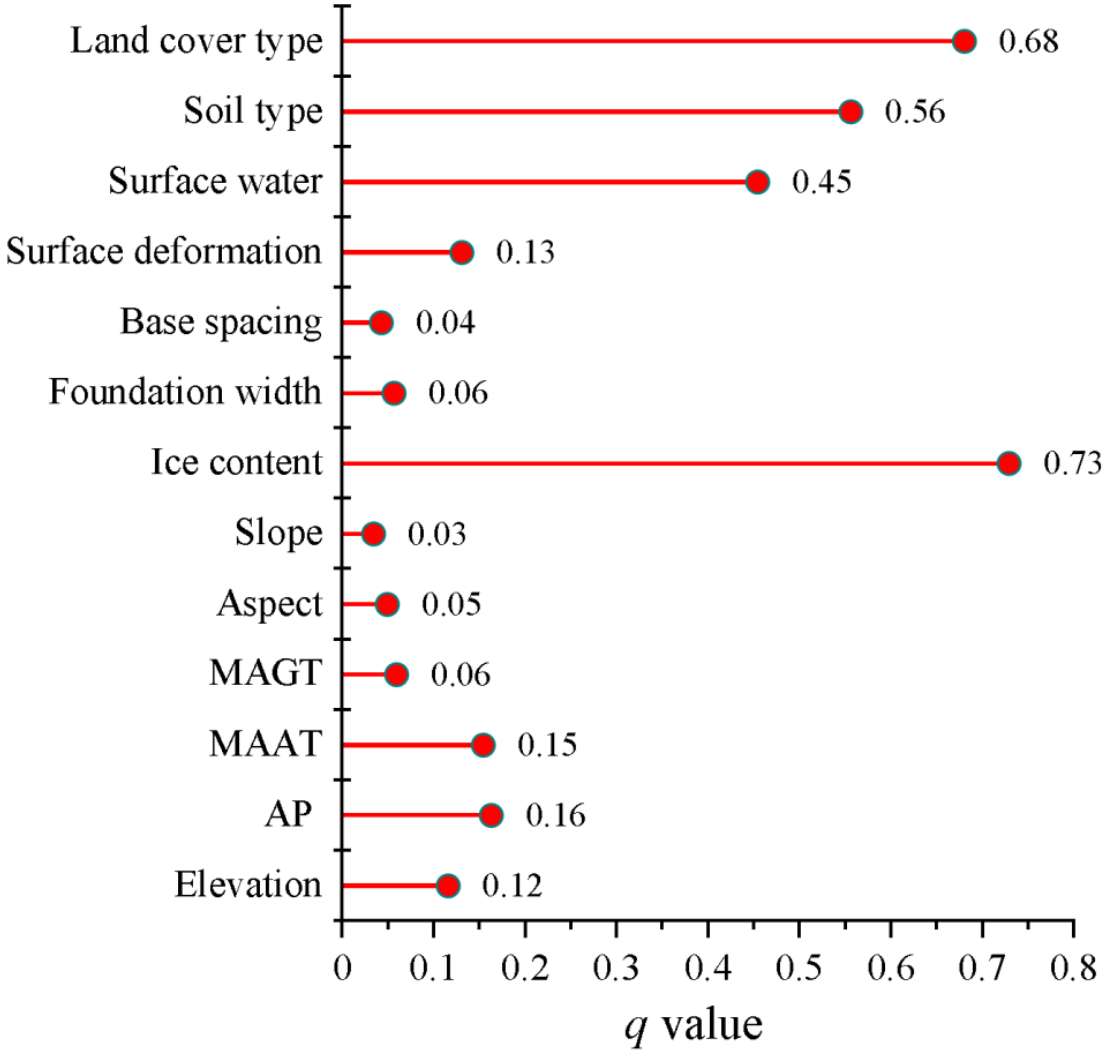


Figure 16. Single-factor detection for frost jacking drivers of transmission tower foundations.

Figure 17 presents the results of the interaction detection analysis. The effects generated by the interaction between any two factors are greater than the effect of a single factor, exhibiting a two-factor enhancement characteristic. This indicates that interactions among factors have a stronger influence on the stability of tower foundations. The magnitude of their combined effects varies significantly. As shown in Figure 17, the strongest explanatory power comes from the interaction between ground ice content and land cover type, achieving a q-value of 0.78. This highlights the importance of considering coupled environmental controls in assessing foundation stability.

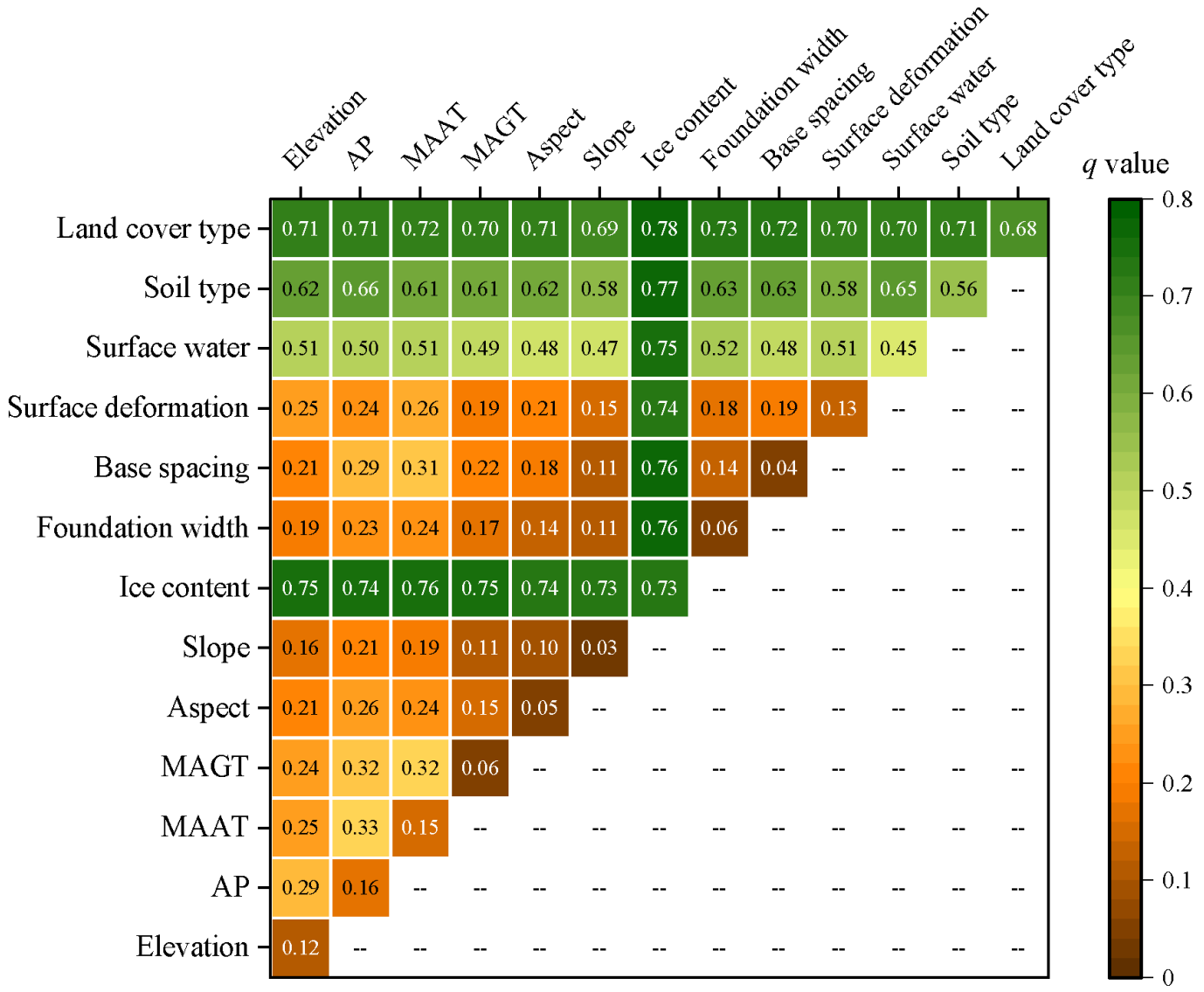


Figure 17. Interactive detection matrix for frost jacking drivers of transmission tower foundations.

4. Conclusions

(1) Within the study-area engineering corridor, differential frost jacking represents the primary structural hazard for transmission tower foundations. Although uniform uplift occurs more frequently (14.3%), non-uniform distress (8.7%) produces larger vertical displacements and correlates positively with tower tilting. Peat-rich wetland geohydrological settings constitute the highest-risk terrain for foundation uplift.

(2) Among the five evaluated ML models, RF achieved the highest observed AUC (0.987) and showed competitive performance across the other evaluation metrics. Its test accuracy, precision, and recall were 0.95, 1, and 0.783, respectively. RF was therefore used for subsequent feature-importance and SHAP analyses.

(3) Ground ice content exhibited the highest explanatory importance for frost-jacking susceptibility across RF feature importance, SHAP attribution, and GeoDetector analysis. Higher ground-ice conditions were generally associated with model predictions toward the frost-jacked class, whereas woodland and gravel-soil conditions were more frequently associated with predictions toward the non-frost-jacked class. The highest joint explanatory power was observed for ground ice content and land cover

(q = 0.78), highlighting the importance of considering multi-factor interactions when evaluating foundation stability.

Author Contributions: Writing—original draft, J.L.; Writing—review and editing, J.L. and G.L.; Validation, J.L.; Investigation, J.L., K.G. and D.C.; Data curation, J.L. and K.G.; Funding acquisition, G.L. and D.C.; Conceptualization, G.L.; Supervision, Y.C. and A.N.F. All authors have read and agreed to the published version of the manuscript.

Funding: This work was funded by the National Natural Science Foundation of China under grant number 42272339; Science & Technology Fundamental Resources Investigation Program, Ministry of Science and Technology of the People's Republic of China under grant number 2022FY100705; Research program for International Research Center for China–Mongolia–Russia Cold and Arid Regions Environment and Engineering, Chinese Academy of Sciences under grant number 121362ZYLH20230002; the program of the State Key Laboratory of Cryosphere Science and Frozen Soil Engineering under grant number CSFSE-ZZ-2406; and the Open Foundation of National Cryosphere Desert Data Center under grant number 2024NCDC006.

Data Availability Statement: The original contributions presented in this study are included in the article. Further inquiries can be directed to the corresponding author.

Conflicts of Interest: The authors declare no conflicts of interest.

Abbreviations

The following abbreviations are used in this manuscript:

AFJA	average frost jacking amount
AP	annual precipitation
AUC	area under the curve
CRCOPs	China–Russia crude oil pipelines
DEM	digital elevation model
EMDSP	Environmental Meteorology Data Service Platform
FPR	false positive rate
GeoDetector	Geographical Detector
LR	Logistic Regression
MAAT	mean annual air temperature
MAGT	mean annual ground temperature
NUFJ	Non-uniform frost jacking
RF	Random Forest
ROC	receiver operating characteristic
SHAP	SHapley Additive exPlanations
SRTM	Shuttle Radar Topography Mission
TPR	true positive rate
TS	Thaw settlement
UAV	unmanned aerial vehicle
UFJ	Uniform frost jacking
XAP	Xing'an permafrost

References

1. Zhang, Z.Q.; Li, M.; Wu, Q.B.; Wang, X.; Jin, H.J.; Chen, H.E.; Ma, D.; Zhang, Z. Degradation and local growth of "Xing'an-Baikal" permafrost responding to climate warming and the consequences. *Earth-Sci. Rev.* **2024**, *255*, 104865. [CrossRef]
2. Jin, H.J.; Yu, Q.H.; Lü, L.Z.; Guo, D.X.; He, R.X.; Yu, S.P.; Sun, G.Y.; Li, Y.W. Degradation of permafrost in the Xing'anling Mountains, northeastern China. *Permafr. Periglac. Process.* **2007**, *18*, 245–258. [CrossRef]
3. Shan, W.; Yang, T.; Guo, Y.; Zhang, C.; Hu, Z.; Wang, Y. Thermohydromechanical coupling analysis and engineering verification of gravel pile groups for strengthening permafrost marshland highway foundations. *Bull. Eng. Geol. Environ.* **2022**, *81*, 294. [CrossRef]

4. Luo, D.; Jin, H.; Jin, R.; Yang, X.; Lü, L. Spatiotemporal variations of climate warming in northern Northeast China as indicated by freezing and thawing indices. *Quat. Int.* **2014**, *349*, 187–195. [CrossRef]
5. Li, X.; Jin, H.; Sun, L.; Wang, H.; He, R.; Huang, Y.; Chang, X. Climate warming over 1961-2019 and impacts on permafrost zonation in Northeast China. *J. For. Res.* **2022**, *33*, 767–788. [CrossRef]
6. Wang, H.; Jin, H.; Che, T.; Li, X.; Dai, L.; Qi, Y.; Huang, C.; He, R.; Zhang, J.; Yang, R.; et al. Influences of snow cover on the thermal regimes of Xing'an permafrost in Northeast China in 1960s–2010s. *Permafr. Periglac. Process.* **2024**, *35*, 188–201. [CrossRef]
7. Mu, Y.H.; Li, G.Y.; Ma, W.; Song, Z.M.; Zhou, Z.W.; Wang, F. Rapid permafrost thaw induced by heat loss from a buried warm-oil pipeline and a new mitigation measure combining seasonal air-cooled embankment and pipe insulation. *Energy* **2020**, *203*, 117919. [CrossRef]
8. Gao, K.; Li, G.; Chen, D.; Su, A.; Cao, Y.; Li, C.; Wu, G.; Du, Q.; Lin, J.; Wang, X.; et al. Pavement damage characteristics in the permafrost regions based on UAV images and airborne LiDAR data. *Cold Reg. Sci. Technol.* **2024**, *228*, 104313. [CrossRef]
9. Lin, J.; Zhang, H.; Li, G.; Su, A.; Wang, X.; Wang, M.; Gao, K.; Chen, D. Properties of ground surface temperature within the Engineering Corridor traversing the Xing'an permafrost region in Northern Northeast China. *Cold Reg. Sci. Technol.* **2025**, *239*, 104589. [CrossRef]
10. Hao, D.; Shi, Y.; Chen, R.; Lu, Z.; Ji, Y.; Lv, Z.; Liu, L. Response of Thermo-Hydro-Mechanical Fields to Pile Material in Pile–Soil System Under Freezing Based on Numerical Analysis. *Buildings* **2025**, *15*, 534. [CrossRef]
11. Grigor'ev, V.S.; Ol'shanskii, V.G.; Starostenkov, A.D.; Khromyshev, N.K.; Shevtsov, K.P. Experience in 110-500 KV overhead transmission line construction and renovation projects in the Northern Regions of Western Siberia. *Power Technol. Eng.* **2012**, *46*, 317–320. [CrossRef]
12. Wang, T.; Qu, S.; Liu, J.; Luo, Q.; Hu, T. Frost jacking of piles in seasonally and perennially frozen ground. *Cold Reg. Sci. Technol.* **2022**, *203*, 103662. [CrossRef]
13. Guo, L.; Yu, Q.; Yin, N.; You, Y.; Wang, J.; Sun, Y.; Chen, K. Two-phase closed thermosyphon-induced frost jacking of piles and foundation instability in a thawed permafrost area. *Nat. Hazards* **2024**, *120*, 619–637. [CrossRef]
14. Zhou, Y.; Wang, X.; Niu, F.; He, F.; Guo, C.; Liu, D.; Jiang, D. Frost jacking characteristics of transmission tower pile foundations with and without thermosyphons in permafrost regions of Qinghai–Tibet plateau. *J. Cold Reg. Eng.* **2021**, *35*, 04021004. [CrossRef]
15. Shang, Y.; Niu, F.; Fang, J.; Wu, L. Experimental study on thermal regime and frost jacking of pile foundation during operation period in permafrost regions. *Front. Earth Sci.* **2022**, *10*, 821305. [CrossRef]
16. Avis, C.A.; Weaver, A.J.; Meissner, K.J. Reduction in areal extent of high-latitude wetlands in response to permafrost thaw. *Nat. Geosci.* **2011**, *4*, 444–448. [CrossRef]
17. Guo, L.; Zhang, Z.; Wang, X.; Yu, Q.; You, Y.; Yuan, C.; Xie, Y.; Gou, T. Stability analysis of transmission tower foundations in permafrost equipped with thermosiphons and vegetation cover on the Qinghai-Tibet Plateau. *Int. J. Heat Mass Transf.* **2018**, *121*, 367–376. [CrossRef]
18. He, P.; Niu, F.; Huang, Y.; Zhang, S.; Jiao, C. Distress characteristics in embankment-bridge transition section of the Qinghai-Tibet railway in permafrost regions. *Int. J. Disaster Risk Sci.* **2023**, *14*, 680–696. [CrossRef]
19. Cao, Y.; Li, G.; Li, C.; Gao, K.; Zhang, H.; Shang, Y.; Sheng, J. Foundation problems of the transmission lines in high latitude permafrost regions and countermeasures: A case study in Northeastern China. *KSCE J. Civ. Eng.* **2025**, *29*, 100283. [CrossRef]
20. Guo, L.; Xie, Y.; Yu, Q.; You, Y.; Wang, X.; Li, X. Displacements of tower foundations in permafrost regions along the Qinghai–Tibet Power Transmission Line. *Cold Reg. Sci. Technol.* **2016**, *121*, 187–195. [CrossRef]
21. Chai, M.; Li, G.; Ma, W.; Cao, Y.; Wu, G.; Mu, Y.; Chen, D.; Zhang, J.; Zhou, Z.; Zhou, Y.; et al. Assessment of freeze-thaw hazards and water features along the China–Russia Crude Oil Pipeline in permafrost regions. *Remote Sens.* **2020**, *12*, 3576. [CrossRef]
22. Kainthura, P.; Sharma, N. Machine learning driven landslide susceptibility prediction for the Uttarkashi region of Uttarakhand in India. *Georisk Assess. Manag. Risk Eng. Syst. Geohazards* **2022**, *16*, 570–583. [CrossRef]
23. Fan, X.; Lin, Z.; Yao, M.; Wang, Y.; Gu, Q.; Luo, J.; Wu, X.; Gao, Z. Spatio-temporal evolution and susceptibility assessment of thaw slumps associated with climate change in the Hoh Xil Region, in the Hinterland of the Qinghai-Tibet Plateau. *Remote Sens.* **2025**, *17*, 1614. [CrossRef]
24. Li, R.; Zhang, M.; Pei, W.; Duan, Z. Integrating thaw settlement hazard and human socio-economic activity for the current and mid-21st century risk evaluation in the Qinghai–Tibet Plateau. *Bull. Eng. Geol. Environ.* **2025**, *84*, 361. [CrossRef]
25. Zhu, H.; Zhang, X.; Wei, G.; Wang, Q.; Liu, X.; Yan, L.; Wang, G. A method for better mapping of susceptibility to thaw hazards in data-scarce cold regions. *Remote Sens. Environ.* **2026**, *337*, 115338. [CrossRef]
26. Li, R.; Zhang, M.; Pei, W.; Melnikov, A.; Zhang, Z.; Li, G. Risk evaluation of thaw settlement using machine learning models for the Wudaoliang–Tuotuohe region, Qinghai–Tibet Plateau. *Catena* **2023**, *220*, 106700. [CrossRef]
27. Zhang, S.; Niu, F.; Wang, S.; Sun, Y.; Wang, J.; Dong, T. Risk assessment of engineering diseases of embankment-bridge transition section for railway in permafrost regions. *Permafr. Periglac. Process.* **2022**, *33*, 46–62. [CrossRef]
28. Lundberg, S.M.; Lee, S.-I. A unified approach to interpreting model predictions. In *Advances in Neural Information Processing Systems 30*; NIPS Foundation: San Diego, CA, USA, 2017; pp. 4768–4777.

29. Lin, Z.; Yan, T.; Shen, S. Multi-criteria analysis combined with machine learning in risk assessment: A Chinese case. *Georisk Assess. Manag. Risk Eng. Syst. Geohazards* **2025**, *19*, 804–823. [CrossRef]
30. Obu, J.; Westermann, S.; Bartsch, A.; Berdnikov, N.; Christiansen, H.H.; Dashtseren, A.; Delaloye, R.; Elberling, B.; Etzelmüller, B.; Kholodov, A.; et al. Northern Hemisphere permafrost map based on TTOP modelling for 2000–2016 at 1 km^2 scale. *Earth-Sci. Rev.* **2019**, *193*, 299–316. [CrossRef]
31. Kwon, K.; Choi, H.; Pham, K.; Kim, S.; Bae, A. Influence analysis of pavement distress on international roughness index using machine learning. *KSCE J. Civ. Eng.* **2024**, *28*, 4344–4355. [CrossRef]
32. Breiman, L. Random forests. *Mach. Learn.* **2001**, *45*, 5–32. [CrossRef]
33. Chen, T.; Guestrin, C. XGBoost: A scalable tree boosting system. In *Proceedings of the 22nd ACM SIGKDD International Conference on Knowledge Discovery and Data Mining, San Francisco, CA, USA*; Association for Computing Machinery: New York, NY, USA, 2016; pp. 785–794.
34. Ke, G.; Meng, Q.; Finley, T.; Wang, T.; Chen, W.; Ma, W.; Ye, Q.; Liu, T. LightGBM: A Highly Efficient Gradient Boosting Decision Tree. In *Advances in Neural Information Processing Systems 30*; NIPS Foundation: San Diego, CA, USA, 2017.
35. Prokhorenkova, L.; Gusev, G.; Vorobev, A.; Dorogush, A.V.; Gulin, A. CatBoost: Unbiased boosting with categorical features. In *Advances* in Neural Information Processing Systems 31; NIPS Foundation: San Diego, CA, USA, 2018.
36. Hosmer, D.W., Jr.; Lemeshow, S.; Sturdivant, R.X. *Applied Logistic Regression*; John Wiley & Sons: Hoboken, NJ, USA, 2013.
37. Lundberg, S.M.; Erion, G.; Chen, H.; DeGrave, A.; Prutkin, J.M.; Nair, B.; Katz, R.; Himmelfarb, J.; Bansal, N.; Lee, S.-I. From local explanations to global understanding with explainable AI for trees. *Nat. Mach. Intell.* **2020**, *2*, 56–67. [CrossRef]
38. Wang, J.; Xu, C. Geodetector: Principle and prospective. *Acta Geogr. Sin.* **2017**, *72*, 116–134. (In Chinese)
39. Yan, A.; Li, S.; Jin, X.; Huang, S.; Wang, W.; Tang, J.; Li, A.Y.; Zhang, Z.; Zhang, S.; Zhai, J.; et al. Multi-source assessment of permafrost deformation along the Bei'an–Hei'he highway in Northeast China. *Remote Sens. Environ.* **2026**, *333*, 115143. [CrossRef]
40. Wang, F.; Li, G.Y.; Ma, W.; Wu, Q.B.; Serban, M.; Vera, S.; Alexandr, F.; Jiang, N.S.; Wang, B. Pipeline-permafrost interaction monitoring system along the China-Russia crude oil pipeline. *Eng. Geol.* **2019**, *254*, 113–125. [CrossRef]
41. Wang, F.; Li, G.; Ma, W.; Chen, D.; Wu, G.; Cao, Y.; Mu, Y.; Mao, Y.; Zhang, J.; Gao, K.; et al. Assessment of permafrost disturbances caused by two parallel buried warm-oil pipelines: A case study at a high-latitude wetland site in Northeast China. *Cold Reg. Sci. Technol.* **2023**, *206*, 103753. [CrossRef]

Disclaimer/Publisher's Note: The statements, opinions and data contained in all publications are solely those of the individual author(s) and contributor(s) and not of MDPI and/or the editor(s). MDPI and/or the editor(s) disclaim responsibility for any injury to people or property resulting from any ideas, methods, instructions or products referred to in the content.